The Role of Nonlinear Forcing Singular Vector Tendency Error in Causing the "Spring Predictability Barrier" for ENSO

DUAN Wansuo[1] (段晚锁), ZHAO Peng[2] (赵 鹏), HU Junya[1,3] (胡均亚), and XU Hui[1*] (徐 辉)

1 *State Key Laboratory of Numerical Modeling for Atmospheric Sciences and Geophysical Fluid Dynamics, Institute of Atmospheric Physics, Chinese Academy of Sciences, Beijing* 100029

2 *China Meteorological Administration Training Center, Beijing* 100081

3 *University of Chinese Academy of Sciences, Beijing* 100049

(Received February 19, 2016; in final form September 5, 2016)

ABSTRACT

With the Zebiak–Cane model, the present study investigates the role of model errors represented by the nonlinear forcing singular vector (NFSV) in the "spring predictability barrier" (SPB) phenomenon in ENSO prediction. The NFSV-related model errors are found to have the largest negative effect on the uncertainties of El Niño prediction and they can be classified into two types: the first is featured with a zonal dipolar pattern of SST anomalies (SSTA), with the western poles centered in the equatorial central–western Pacific exhibiting positive anomalies and the eastern poles in the equatorial eastern Pacific exhibiting negative anomalies; and the second is characterized by a pattern almost opposite to the first type. The first type of error tends to have the worst effects on El Niño growth-phase predictions, whereas the latter often yields the largest negative effects on decaying-phase predictions. The evolution of prediction errors caused by NFSV-related errors exhibits prominent seasonality, with the fastest error growth in spring and/or summer; hence, these errors result in a significant SPB related to El Niño events. The linear counterpart of NFSVs, the (linear) forcing singular vector (FSV), induces a less significant SPB because it contains smaller prediction errors. Random errors cannot generate an SPB for El Niño events. These results show that the occurrence of an SPB is related to the spatial patterns of tendency errors. The NFSV tendency errors cause the most significant SPB for El Niño events. In addition, NFSVs often concentrate these large value errors in a few areas within the equatorial eastern and central–western Pacific, which likely represent those areas sensitive to El Niño predictions associated with model errors. Meanwhile, these areas are also exactly consistent with the sensitive areas related to initial errors determined by previous studies. This implies that additional observations in the sensitive areas would not only improve the accuracy of the initial field but also promote the reduction of model errors to greatly improve ENSO forecasts.

Key words: spring predictability barrier, model error, optimal perturbation, El Niño event

Citation: Duan Wansuo, Zhao Peng, Hu Junya, et al., 2016: The role of nonlinear forcing singular vector tendency error in causing the "spring predictability barrier" for ENSO. *J. Meteor. Res.*, **30**(6), 853–866, doi: 10.1007/s13351-016-6011-4.

1. Introduction

The El Niño–Southern Oscillation (ENSO), a large-scale interannual fluctuation caused by interactions between the atmosphere and the ocean over the tropical Pacific, has great climatic and socioeconomic impacts worldwide (McPhaden et al., 2006). Understanding of ENSO and its predictions are therefore important and have received tremendous attention over the years. Despite continuous improvements in ENSO models and predictions in recent decades, realistic ENSO predictions still contain considerable uncertainties (Kleeman, 1991; Latif et al., 1994, 1998; Luo et al., 2008; Jin et al., 2008). Even in predicting the years 2014/2015, most models encounter significant challenges and provide false alerts for El Niño occurrences. Moreover, most models successfully forecast the occurrence of 2015/2016 El Niño events, but

Supported by the China Meteorological Administration Special Public Welfare Research Fund (GYHY201306018), National Natural Science Foundation of China (41230420 and 41525017), and National Program on Global Change and Air–Sea Interactions (GASI-IPOVAI-06).

*Corresponding author: xuh@lasg.iap.ac.cn.

the predicted intensities contain large uncertainties. The challenge in forecasting ENSO events may be related to the "spring predictability barrier" (SPB), which means that ENSO predictions tend to be much less reliable when the forecasts are made before or during the spring.

The SPB is a critical component of ENSO forecasts (Webster and Yang, 1992; Lau and Yang, 1996; McPhaden, 2003), but its origin is still debatable. Quite a few studies have attempted to explain this phenomenon (Penland and Magorian, 1993; Webster, 1995; Moore and Kleeman, 1996; Torrence and Webster, 1998; Samelson and Tziperman, 2001; McPhaden, 2003; Levine and McPhaden, 2015). Particularly, most highlight the role of initial errors in yielding a "significant SPB."

In terms of prediction error growth, a "significant SPB" means that ENSO predictions do not only contain a significantly large prediction error but also exhibit prominent error growth during the boreal spring when these predictions are made before or throughout the season. Moore and Kleeman (1996) investigated the SPB by using the singular vector approach, which represents the fastest growing initial errors in a linear model. Chen et al. (2004) suggested that the improvement of the model initialization procedure could reduce and even eliminate this predictability barrier phenomenon. Zheng and Zhu (2010) also showed the importance of reducing initial errors in improving a model's ENSO forecast ability. Particularly, Mu et al. (2007a, b) applied the conditional nonlinear optimal perturbation (CNOP) approach (Mu et al., 2003) to ENSO predictability and showed that the SPB occurs as a result of the combined effect of climatological seasonal cycles, El Niño, and the initial error structure. For a given model, the first two factors are inherent (Stein et al., 2010; Dommenget and Yu, 2016), and the seasonality of error growth usually originates from them. Along these lines, the results of Mu et al. (2007a, b) indicated that particular initial error patterns could determine whether an SPB is present (Duan et al., 2009). Yu et al. (2009) revealed the initial error most likely to generate a significant SPB for El Niño events; particularly, they showed how SPB-related initial errors exist in realistic predictions (Duan et al., 2009; Duan and Wei, 2012). Furthermore, when the SPB-related initial errors are filtered out, ENSO model forecast ability is greatly improved (Duan and Hu, 2016).

Gebbie and Tziperman (2009) found that integrating westerly wind bursts (WWBs) improved their prediction of the onset and development of the exceptionally large 1997 El Niño event, suggesting a potential for ENSO prediction improvements within the SPB. Lopez and Kirtman (2014) also showed that including state-dependent WWBs in a fully coupled prediction model significantly increased their model's ENSO prediction ability. These two studies indicate that when a model fails to address the effect of WWBs and yields model errors, the ability of that model to forecast ENSO events is also largely influenced. For example, Yu et al. (2003) suggested that the characteristics of WWBs depend on the large-scale SST field and are therefore not purely stochastic, which implies that the model errors induced by the lack of WWBs may be of a certain structure and have a large effect on ENSO prediction errors. In realistic predictions, model errors may include not only atmospheric variability forcing uncertainties but also model parameterizations and boundary condition uncertainties (Blanke et al., 1997; Flügel and Chang, 1998; Latif et al., 1998; Liu, 2002; Mu et al., 2002; Zhang et al., 2003; Zavala-Garay et al., 2004; Williams, 2005; Duan and Zhang, 2010; Yu et al., 2012a). Furthermore, it is very difficult to separate these uncertainties' respective roles in overall prediction uncertainty. The combined effect of these kinds of model errors must be investigated. As a consequence, we ask: how can we study the combined effect of groups of model errors? Do such model errors have a particular pattern, and does that pattern cause significant prediction uncertainty? Can these errors induce the SPB associated with ENSO predictions? And, how can researchers reduce the effect of model errors on ENSO forecasts? In this paper, we address these questions. In Section 2, we introduce the approach. In Section 3, we introduce the Zebiak–Cane model adopted in this study and highlight the model errors that have the largest effect on ENSO predictions. In Section 4, the role of these model errors on the SPB phenomenon is explored. Section 5 explores

the dependence of SPB to El Niño event predictions on the spatial structure of tendency errors. Section 6 discusses the implication of the featured model errors associated with the SPB. Finally, a summary of the main results and discussion are presented in Section 7.

2. Approach: nonlinear forcing singular vector

Model errors generally stem from a combination of uncertainties in discrete and subgrid-scale numerical parameterization schemes (Syu and Neelin, 2000), the representation of intraseasonal atmospheric variability (Marshall et al., 2009), model boundary conditions, etc (Wu et al., 1993). Therefore, the effects of these types of model errors are mixed; and it is very difficult to distinguish their respective roles in yielding prediction uncertainties. Roads (1987) used tendency errors to approximate the combined effect of different types of model errors and expressed the model in the form

$$\frac{\partial \boldsymbol{U}}{\partial t} = F(\boldsymbol{U}(\boldsymbol{x};t)) + \boldsymbol{f}, \tag{1}$$

where the function $F(\boldsymbol{U}(\boldsymbol{x};t))$ is the model equation tendency, and $\boldsymbol{f}$ is a forcing term, which can be computed by assimilating the observations. Within the Roads' procedure, the forcing $\boldsymbol{f}$ can be roughly identified as responsible for processes that are omitted or mistreated by the model equation (Roads, 1987; McCreary and Anderson, 1991; Barkmeijer et al., 2003). Following this study, Barkmeijer et al. (2003) assumed perfect initial conditions and introduced the (linear) forcing singular vector (FSV) approach to describe the constant tendency perturbation resulting in considerable perturbation growth within a linear model during a predetermined forecast period.

The motions of the atmosphere, ocean, and their coupled system (e.g., ENSO) are often dominated by complex nonlinear systems. The FSV is therefore limited in its ability to show its effect on tendency errors within nonlinear physical processes. To overcome this limitation, Duan and Zhou (2013) introduced the nonlinear forcing singular vector (NFSV) approach. An NFSV is the tendency perturbation that generates the largest prediction error in the reference state to be predicted in a nonlinear model at the prediction time based on physical constraint conditions. To assist the readers, we review the NFSV approach briefly below.

For a measurement $\|\cdot\|$, a tendency perturbation $\boldsymbol{f}_\delta$ is called an NFSV if and only if

$$J(\boldsymbol{f}_\delta) = \max_{\|\boldsymbol{f}\|_a \leqslant \delta} \|\boldsymbol{M}_{t_0,t_k}(\boldsymbol{f})(\boldsymbol{U}_0) - \boldsymbol{M}_{t_0,t_k}(0)(\boldsymbol{U}_0)\|_b, \tag{2}$$

where $\|\cdot\|_a$ and $\|\cdot\|_b$ measure the amplitude of the tendency error $\boldsymbol{f}$ and its resultant prediction error, respectively. These values can be the same or different, depending on the physical problem of interest. The variable $\boldsymbol{f}$ is subject to the constraint radius δ; $\boldsymbol{M}_{t_0,t_k}(\boldsymbol{f})$ is the propagator of a nonlinear model with tendency error $\boldsymbol{f}$ from initial time t_0 to prediction time t_k; and $\boldsymbol{U}_0$ is the initial value of the reference state and we do not consider its errors in predictions in this study.

The linear FSV is as follows:

$$\lambda(\boldsymbol{f}^*) = \max_{\boldsymbol{f}} \frac{\|\boldsymbol{M}_\tau(\boldsymbol{f})(0)\|}{\|\boldsymbol{f}\|}, \tag{3}$$

where $\boldsymbol{M}_\tau(\boldsymbol{f})$ is the tangent linear operator of $\boldsymbol{M}_\tau(\boldsymbol{f})$; the inner product is chosen to describe the norm $\|\cdot\|$ here. By solving the optimization problem in Eq. (3), the FSV can be obtained. The FSV represents the tendency perturbation that causes the largest perturbation growth during the forecast period in a linear sense.

Obviously, if we regard the tendency perturbation as the tendency error in predictability studies, the NFSVs, compared to the FSVs, are much applicable in describing the tendency error that causes the largest error growth in the perfect initial condition scenario. In this paper, we will use the NFSV approach to explore the role of model error in causing SPBs related to El Niño events and compare these errors with the FSV, finally revealing the effect of nonlinearity and providing implications for reducing model errors.

3. The model error characterized by the NFSV in the Zebiak–Cane model

3.1 The Zebiak–Cane model

The Zebiak–Cane model is the first coupled atmosphere–ocean model to successfully simulate ENSO variability. It is an intermediate nonlinear

anomaly model that describes the evolution of anomalies with respect to a prescribed seasonally varying background flow. Since 1986, the Zebiak–Cane model has been used to conduct realistic ENSO forecasting and was well known for successfully predicting the onset of the 1991/1992 El Niño event. Owing to its good performance, it has been widely applied in ENSO prediction and predictability studies (Zebiak and Cane, 1987; Blumenthal, 1991; Xue et al., 1994; Chen et al., 1995, 2004; Mu et al., 2007a; Tang et al., 2008; Duan et al., 2009). The model consists of a Gill-type steady-state linear atmospheric model with a horizontal resolution of 5.625° × 2.0° and a reduced-gravity oceanic model with a horizontal resolution of 2.0° × 0.5°. These depict the anomalous thermodynamics and dynamics of ocean–atmospheric interactions over the tropical Pacific (Zebiak and Cane, 1987).

3.2 The NFSVs of the Zebiak–Cane model associated with El Niño events

To obtain NFSVs in the Zebiak–Cane model, we predetermine the reference-state El Niño events to be predicted from the 1000-yr integration model. In the Zebiak–Cane model, if Niño-3 indices (the SSTA averaged over Niño-3 region) greater than 0.5℃ persist for more than six months, an El Niño event is identified. There are numerous El Niño events with different intensities that occur over the 1000-yr timeframe and have a dominant period of 4 yr. Similar to Duan et al. (2009), the 1000 model years in the present study are divided into 10 continuous time intervals beginning with 0–99, 100–199 yr, and so on. In each of these 10 time intervals, two groups of model El Niño events are selected: One group consists of 4 strong events with Niño-3 indices (SSTA averaged at 5°N–5°S, 150°–90°W) greater than 2.5℃, denoted by S1, S2, S3, and S4; the other group contains 4 weak events with Niño-3 indices smaller than 2.5℃, which are denoted as W1, W2, W3, and W4. The S1–S4 events initially begin warming in January, April, July, and October, as do the W1–W4 events, respectively. Because similar results are obtained for different time intervals, we randomly selected the two groups of El Niño events during the 100–199-yr period as examples to investigate the effect of model errors on the SPB. The time series of Niño-3 SSTA for these two groups of El Niño events is plotted in Fig. 1. In this paper, the year the reference-state El Niño event peaks is denoted as year (0), and years (–1) and (1) are used to represent the years before and after year (0), respectively. All of the events tend to persist for more than 20 months and peak at the end of the calendar year, similar to observed El Niño events (Fig. 1). Next, we calculate the NFSVs of these El Niño events, that is, the errors that have the largest influence on the El Niño events.

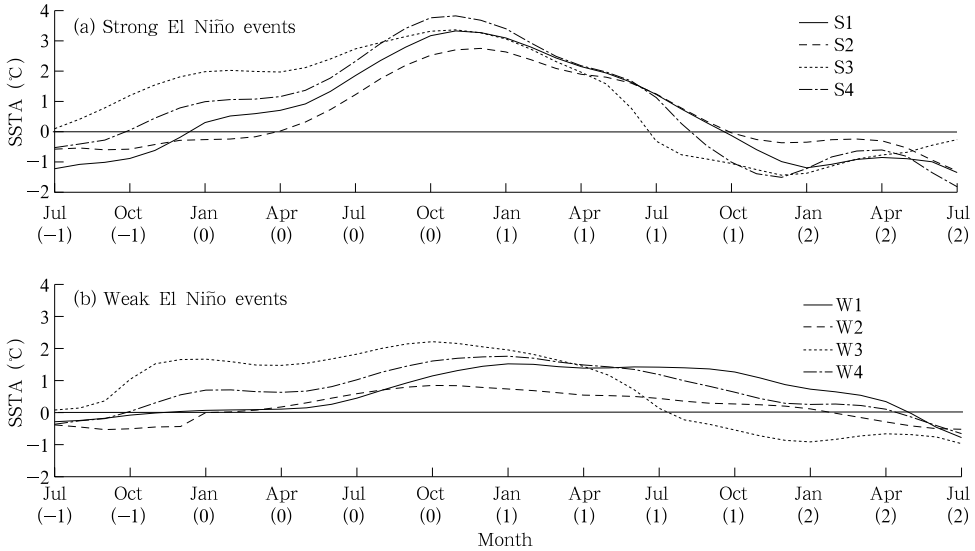

Fig. 1. Time series of Niño-3 SSTA for the (a) strong El Niño events, denoted as S1–S4, and (b) weak El Niño events, denoted as W1–W4.

According to the definition of the NFSV expressed in Eq. (2), we construct the corresponding cost function associated with the NFSV as follows:

$$J(\boldsymbol{f}_\delta) = \max_{\|\boldsymbol{f}\|_a \leqslant \delta} \|T'(t_k)\|_b, \tag{4}$$

where the norm $\|\boldsymbol{f}\|_a = \sqrt{\sum_{i,j}(\boldsymbol{f}_{i,j})^2}$ and $\|T'(t_k)\|_b = \sqrt{\sum_{i,j}(T'_{i,j}(t_k))^2}$ is used to constrain the amplitude (values of δ) of the tendency error $\boldsymbol{f}$ and measure the prediction error caused by $\boldsymbol{f}$; $T'(t_k)$ represents the SSTA prediction errors caused by tendency errors $\boldsymbol{f}$ at prediction time t_k, which is defined as the difference between the predicted SSTA generated by the Zebiak–Cane model superimposed by $\boldsymbol{f}$ at t_k and the SSTA of the reference-state El Niño events; and $T'_{i,j}$ represents the SSTA prediction error at grid point (i, j), which covers the tropical Pacific Ocean of 19°S–19°N, 129.375°E–84.375°W.

Empirically, the constraint bound in Eq. (4) is set at 0.4. A prediction for the preceding 12 months is made for each reference-state El Niño event, starting in Jul (–1) (i.e., Jul in year (–1)), Oct (–1), Jan (0), Apr (0), Jul (0), Oct (0), Jan (1), and Apr (1). For each start month, the El Niño will be predicted by using the Zebiak–Cane model with the SSTA equation perturbed by the error. As a result, each El Niño event will have 8 predictions for a total of 64 predictions across 8 El Niño events. For each prediction, we subtract the SSTA component of the reference-state El Niño event from the resultant El Niño prediction and then obtain the prediction errors caused by the tendency error. Along these lines, we use Eq. (4) to compute the NFSV that causes the largest prediction error. The predictions with Jul (–1), Oct (–1), Jan (0), and Apr (0) start dates cover the spring season of the growth phase of the reference state El Niño events. For convenience, we hereafter call them as growth-phase predictions and the obtained NFSVs as these of the growth-phase predictions. Similarly, the predictions with the start month of Jul (0), Oct (0), Jan (1), and Apr (1) pass through the decay phase of El Niño events and are referred as decaying-phase predictions; then the NFSVs obtained are represented as the ones of the decaying-phase predictions.

The results show that for each prediction, there exists only one NFSV to perturb the SSTA tendency, which often exhibits a large-scale zonal dipolar pattern. Specifically, the NFSVs for the growth-phase predictions with start months Jul (–1), Oct (–1), Jan (0), and Apr (0) are similar and present a zonal SSTA dipole mode with its western poles exhibiting positive anomalies and the eastern poles exhibiting negative anomalies and are denoted as NFSV1 tendency errors (Fig. 2). Meanwhile, the NFSVs of the decaying-phase predictions with the start months Jul (0), Oct (0), Jan (1), and Apr (1) are inclined to have a different zonal dipolar structure, which is nearly opposite that of the growth-phase NFSV and is referred to as NFSV2 tendency error (Fig. 2).

NFSV is a nonlinear generalization of the linear FSV. To compare NFSVs with FSVs and show the nonlinear effect, we calculate the FSVs of the 64 predictions and scale them to ensure that they have the same magnitude as the NFSVs. The results indicate that the FSVs possess a similar, large-scale zonal dipolar structure, except that the FSVs tend to extend their western pole center much farther eastward than the NFSVs. We note that, due to the linearity of FSVs, the negative pattern of an FSV is also an FSV of the events (Duan and Zhao, 2015). Accordingly, we denote FSVs with the same sign as NFSV1 using FSV1, and those with an opposite sign as FSV2. We find that both the FSV1 and NFSV1 are inclined to yield negative prediction errors for Niño-3 SSTA related to El Niño events; while the FSV2 and NFSV2 tend to result in positive prediction errors for the Niño-3 SSTA. Nevertheless, compared with the corresponding NFSVs, the FSVs often lead to a smaller prediction error. All of these results support those obtained in Duan and Zhao (2015), despite the fact that the present study selected a different magnitude of tendency perturbations (the details are therefore omitted here). Considering that the NFSVs cause much larger prediction errors than the FSVs, we suggest that the NFSVs are more likely than the FSVs to cause a significant SPB for El Niño events according to the definition of a significant SPB (see the introduction). To confirm this, we investigate the role of tendency errors

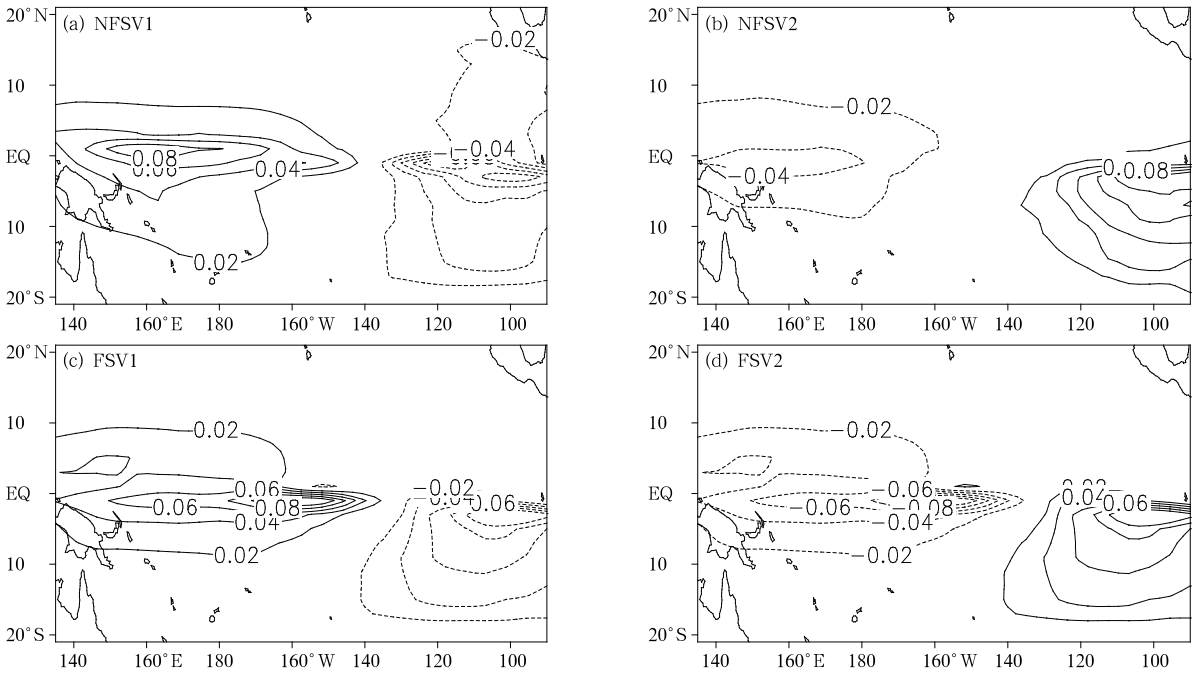

Fig. 2. (a) NFSV1 and (c) FSV1 tendency errors associated with a start month of Jan (0); (b) NFSV2 and (d) FSV2 tendency errors associated with a start month of Jan (1). These NFSVs and FSVs correspond to the reference-state El Niño event denoted as S1.

in causing SPBs in the next section.

4. The role of NFSV-related tendency errors in inducing a significant SPB for El Niño events

As the introduction states, a "significant SPB" refers to the phenomenon that the El Niño prediction has a conspicuous prediction error, and prominent error growth occurs during the boreal spring when the prediction is made before that season. Therefore, we examine the role of tendency errors in SPBs from two perspectives: prediction errors induced by tendency errors and the seasonality of the evolution of those prediction errors. From the definition of NFSV described in Eq. (2), the NFSV tendency errors result in the largest prediction error at the prediction time. Hence, the NFSV errors have the potential to induce a significant SPB phenomenon associated with El Niño events.

To study the seasonality of the evolution of prediction errors caused by NFSV errors, a calendar year was divided into four seasons: spring (April–June: AMJ), summer (July–September: JAS), autumn (October–December: OND), and winter (January–March: JFM). The seasonal growth rate of the prediction errors caused by the NFSV errors is denoted by , which is defined as:

$$\kappa \approx (\|T'(t_2)\|_2 - \|T'(t_1)\|_2)/(t_2 - t_1), \tag{5}$$

where $\|T'(t_1)\|_2$ and $\|T'(t_2)\|_2$ represent the prediction errors of the SSTA fields at the beginning and end of each season, respectively; and $\|T'(t_k)\|_2 = \sqrt{\sum_{i,j}(T'_{i,j}(t_k))^2}(k = 1, 2)$ has the same meaning as in Eq. (4). κ is used to measure the magnitude of the error growth in unit intervals. Supposing every season has the same time span, we represent κ as $\|T'(t_2)\|_2 - \|T'(t_1)\|_2$ for convenience. A positive (negative) κ value implies that the prediction errors increase (decrease) during the relevant season; the larger the absolute κ, the faster the increase (decrease) in the prediction errors associated with that season. Here, since we consider perfect initial conditions, the prediction errors are only caused by tendency errors and their related seasonal growth rates κ are then merely for the tendency error growth.

Samelson and Tziperman (2001) emphasized the effect of different phases of ENSO on SPB from the perspective of initial error growth (also see Yu et al., 2009). Thus, if the errors also induce an SPB, there may be a possibility that the occurrence of an SPB depends on the phase of the El Niño event. Therefore, in the next sections we will investigate the seasonal dependence of resultant prediction errors based on growth-phase predictions and decaying-phase predictions, respectively. We find that the following results hold for either strong or weak events. As a result, we present the results using the combined mean of the prediction errors and their seasonal growth rates for eight El Niño events, but we do not distinguish between the events' intensities.

4.1 Growth-phase predictions of El Niño events

As mentioned in Section 3, the predictions with a start month of Jul (–1), Oct (–1), Jan (0), and Apr (0) are growth-phase predictions for El Niño events. These predictions cover the boreal spring and the beginning of summer (i.e., AMJ and JAS; see Mu et al., 2007a), which correspond to those seasons in which the SPB often occurs in most climate models. Using these four start months, we integrate the Zebiak–Cane model with the corresponding NFSV tendency errors, i.e., NFSV1 tendency errors, and obtain the seasonal growth rate κ (measured by Eq. (5)) of the prediction errors for the eight El Niño events shown in Fig. 1.

Figure 3 shows the ensemble mean of the seasonal growth rates κ of the prediction errors caused by the NFSV1 tendency errors for the growth-phase predictions of each El Niño event, respectively. It is obvious that the prediction errors caused by the NFSV1 tendency errors tend to grow rapidly in spring for start months Jul (–1) and Oct (–1) and in summer for start months Jan (0) and Apr (0). As argued in Mu et al. (2007a), although the maximum error growth of the latter two start months appears in JAS, the error growth during AMJ becomes aggressively large, which could have caused the dramatic decrease in the El Niño forecast ability during AMJ and resulted in an SPB. From the perspective of Mu et al. (2007a), this error growth behavior indicates that the NFSV1 tendency errors tend to yield significant SPBs for El Niño events during growth-phase predictions.

As a comparison, we also calculate the seasonal growth rate of prediction errors caused by corresponding FSV tendency errors (i.e., the FSV1 tendency errors) in growth-phase predictions. The results show that, except for start month Jul (–1), the FSV1 errors tend to grow fastest in spring or summer (in the latter,

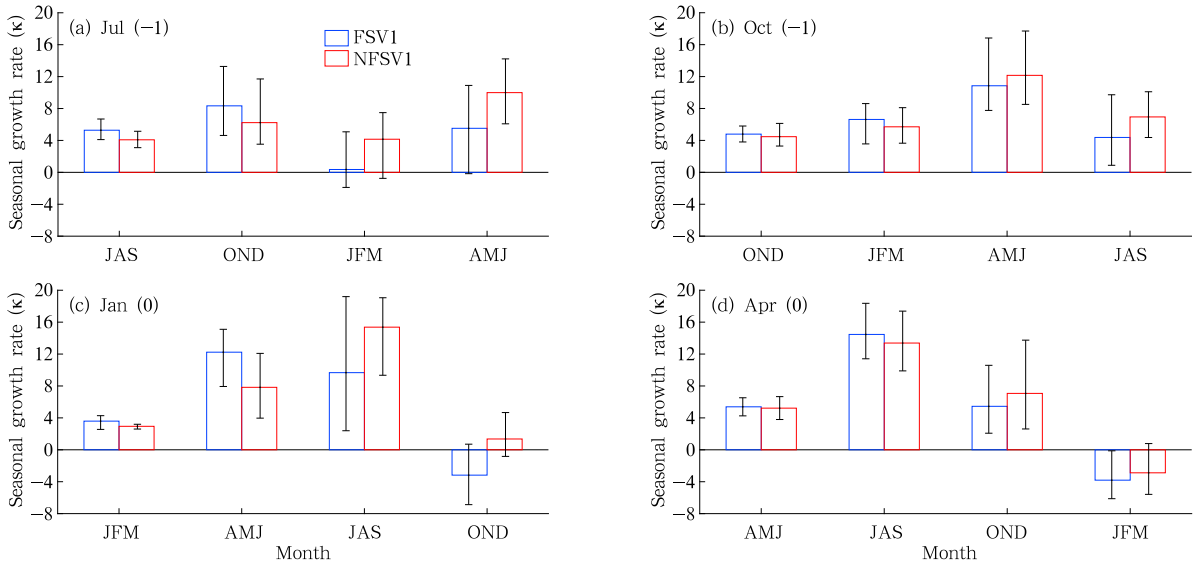

Fig. 3. Combined mean of seasonal growth rate for prediction errors caused by NFSV1 and FSV1 tendency errors in eight reference-state El Niño events. The predictions begin in (a) Jul (–1), (b) Oct (–1), (c) Jan (0), and (d) Apr (0).

the AMJ error growth becomes aggressively large) and induce an SPB. Furthermore, FSV1 tendency error growth dominates the seasonal errors over shorter lead times, while NFSV1 tendency error growth dominates those with longer lead times. Although the FSV1 tendency errors have larger seasonal error growth over shorter lead times, the NFSV1 tendency error dominates subsequent seasonal error growth, especially AMJ and/or JAS error growth, with its larger amplitude, which suggests that the NFSV1 causes larger prediction errors (Fig. 4). Along those lines, if the FSV tendency errors cause smaller prediction errors than the NFSV tendency errors, the FSV errors may induce a less significant SPB to El Niño growth-phase predictions.

4.2 Decaying-phase predictions of El Niño events

Predictions with a start month of Jul (0), Oct (0), Jan (1), and Apr (1) are referred to as decaying-phase predictions; they are made during the boreal spring and beginning of summer during the El Niño decaying phase. To explore whether the corresponding errors cause an SPB to decaying-phase predictions, we calculated the seasonal growth rates of the prediction errors caused by NFSV2 and FSV2 tendency errors (see Section 3). The NFSV2 tendency errors often exhibited a season-dependent evolution, with significant error growth occurring in AMJ and/or JAS and, consequently, resulting in an SPB (Fig. 5). In particular, the error growth associated with the NFSVs is almost always larger than that associated with the FSVs in the AMJ and/or JAS seasons, resulting in a more significant SPB.

Comparing the decaying-phase predictions and the growth-phase predictions (see Figs. 4 and 6), we find that the NFSV tendency errors within growth-phase predictions usually cause larger prediction errors than those within decaying-phase predictions. It follows that the growth-phase predictions are more likely

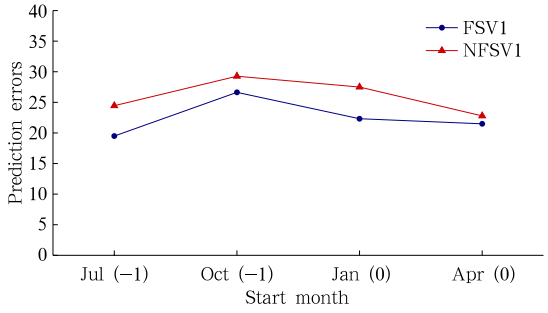

Fig. 4. Averaged prediction errors caused by NFSV1 and FSV1 tendency errors for the eight reference-state El Niño events with start months of Jul (–1), Oct (–1), Jan (0), and Apr (0), and a lead time of 12 months in all cases. Here, the prediction errors are equivalent to the sum of the seasonal growth rates.

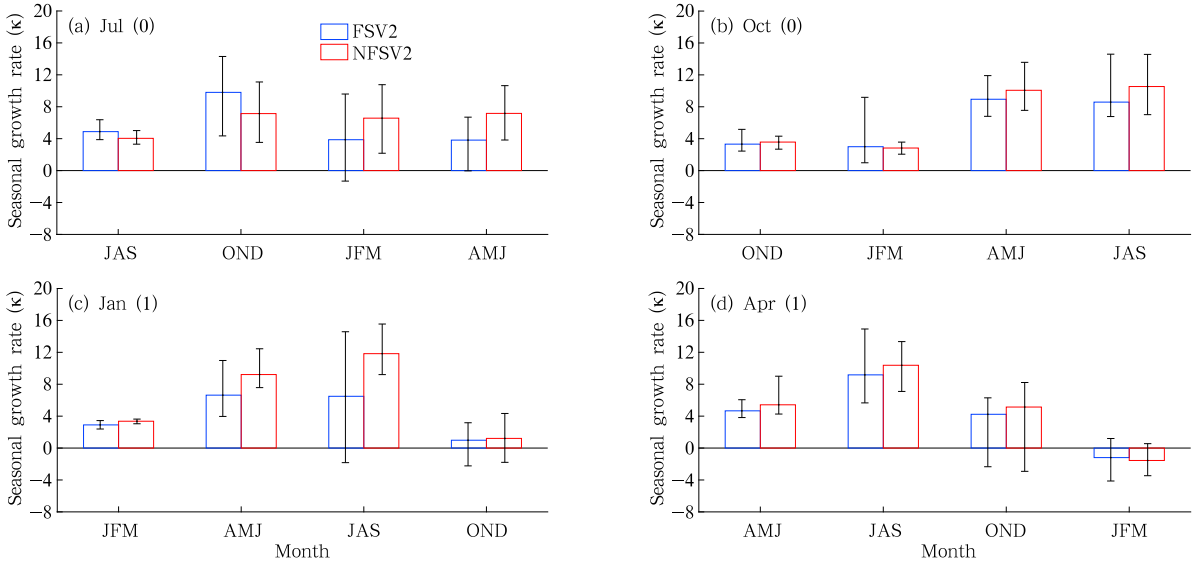

Fig. 5. As in Fig. 3, but for predictions with start months of (a) Jul (0), (b) Oct (0), (c) Jan (1), and (d) Apr (1).

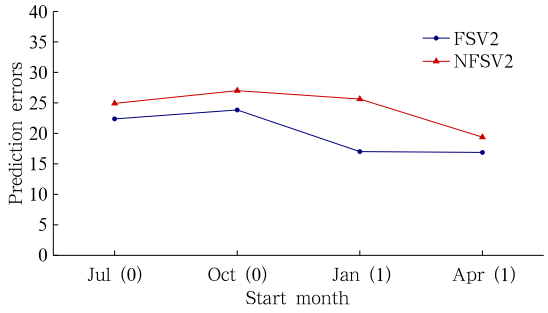

Fig. 6. As in Fig. 4, but for predictions with start months of Jul (0), Oct (0), Jan (1), and Apr (1).

to be contaminated by tendency errors than the decaying-phase predictions. Dommenget et al. (2013) showed that La Niña is more predictable than El Niño. Because the growth phase of La Niña is closely linked to the decaying phase of El Niño, Dommenget et al. (2013) can be argued to support the perspective that decaying-phase predictions of El Niño are more predictable than growth-phase predictions. In addition, Kirtman et al. (2002) stated that ENSO predictions initialized in the spring tend to have more forecast ability than predictions begun in other seasons. Our results also show that predictions begun in April either in the growth or decaying phase of El Niño events always have much small prediction errors compared with those started during other seasons, which indicates that ENSO predictions starting from the boreal spring are more accurate.

5. The dependence of SPB to El Niño event predictions on the spatial structure of tendency errors

NFSV tendency errors result in much larger prediction errors than FSV errors and tend to yield more significant SPBs, which implies that the SPB of El Niño events is sensitive to the spatial structure of tendency errors. That is, those errors with a particular structure tend to cause much larger prediction errors. To further address this issue, we selected random tendency errors without a specific structure. Eight random tendency errors were generated for each reference state El Niño event; the tendency errors at each grid point of the SSTA fields in the Zebiak–Cane model satisfy a normal distribution. To guarantee that the random tendency errors had the same magnitude as the NFSVs, we scaled these random tendency errors by using the function $\boldsymbol{f}_r = \sigma \dfrac{\boldsymbol{f}_R}{\|\boldsymbol{f}_R\|_2}$, where σ is a positive real number equal to the constraint radius (exactly, value of δ is 0.4) of the NFSVs; $\boldsymbol{f}_R$ represents the random tendency error and $\boldsymbol{f}_r$ is the scaled random tendency error, which has the same magnitude as the NFSVs.

By superimposing the random tendency errors on the Zebiak–Cane model, we were able to investigate the resultant prediction errors and related seasonal growth rate. For both the growth-phase and decaying-phase predictions of El Niño events, the random tendency errors cause fairly small prediction errors; furthermore, the error growth at each season is trivial. In Fig. 7, we show the seasonal growth rate of the prediction errors caused by random tendency errors for the growth-phase predictions alone. The random tendency errors have a negligible growth rate during each season and do not exhibit a season-dependent evolution, which results in very small prediction errors and no SPB phenomenon.

The analysis above indicates that random tendency errors do not cause SPBs to El Niño predictions, while FSV tendency errors cause less significant SPBs; and NFSV tendency errors yield significant SPBs. Thus, the NFSV errors cause the most uncertainty in El Niño predictions. These results indicate that the SPB phenomenon caused by tendency errors is highly dependent on the spatial structure of the tendency errors.

6. Implications

NFSVs cause the most disturbing tendency errors in ENSO predictions within the Zebiak–Cane model. That is, the tendency errors with an NFSV structure can more easily yield large uncertainty in El Niño predictions. Particularly, tendency errors characterized by NFSVs are often concentrated in the equatorial central–western and eastern Pacific, which may imply that the errors resulting from these areas contribute to the majority of prediction errors compared with those in other areas. In this sense, if we can improve the

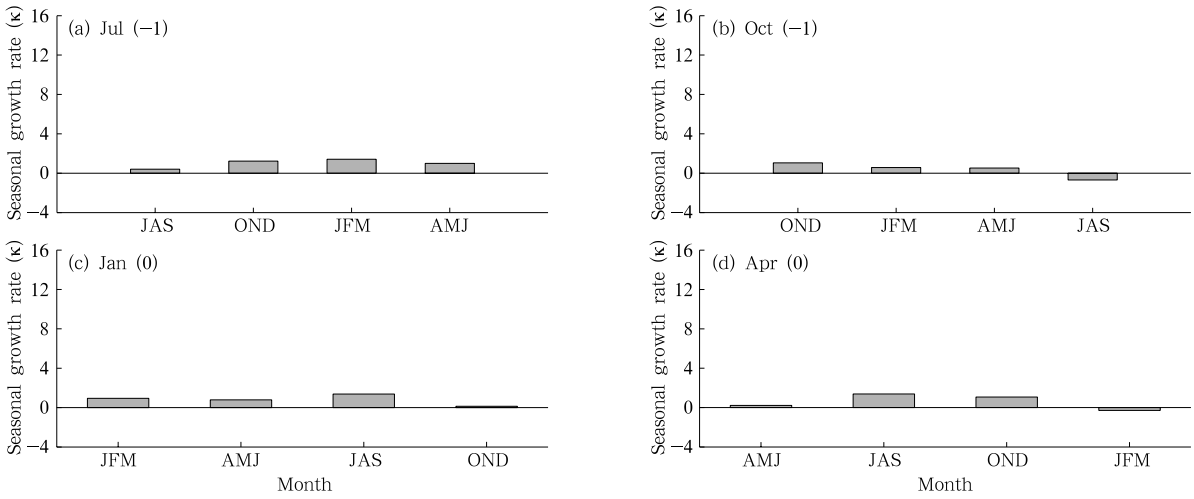

Fig. 7. The combined mean of the seasonal growth rate κ of the prediction errors caused by the random tendency errors for the growth phase predictions, with start months of (a) Jul (–1), (b) Oct (–1), (c) Jan (0), and (d) Apr (0).

model's ability to simulate climatic conditions in these areas, ENSO forecasting may be greatly improved. These areas may represent regions where El Niño predictions are sensitive to model errors. By contrast, FSVs identify sensitive areas within the equatorial central–eastern and eastern Pacific mainly because the western poles of these vectors move farther eastward than those of NFSVs. The difference in the sensitive areas between these two methods is due to the impact of nonlinearity. FSVs are obtained by using a linear scenario and are an approximation of NFSVs (Duan and Zhou, 2013), while NFSVs are generated by using a nonlinear model without any approximation. Therefore, NFSVs are likely more applicable in determining areas where the model is sensitive to errors. That is to say, the areas of sensitivity determined by the NFSVs may be more helpful in proposing significant improvements to the model and, therefore, its ENSO forecast ability.

Duan et al. (2009) and Mu et al. (2014) demonstrated that the equatorial central–eastern Pacific and eastern Pacific represent areas sensitive to initial errors in predicting ENSO events (Yu et al., 2012b), which suggests that taking additional observations in these areas and assimilating them into the initial data will improve model ENSO forecasting more significantly than increasing observations in other areas. Moreover, the present study further shows that prediction errors are also most sensitive to model errors in these sensitive areas. Therefore, improved observation networks in these sensitive areas relative to other areas will not only provide a more accurate initial field of data but also improve our understanding of ENSO physics to optimize ENSO models, thus greatly improving our ENSO forecasting ability.

7. Summary and discussion

This study investigated the role of model errors, as represented by NFSV tendency errors, in inducing SPBs to ENSO predictions within the Zebiak–Cane model. The results show that two types of NFSV tendency errors exist and are associated with growth-phase and decaying-phase predictions of ENSO, respectively. The NFSV1 tendency errors in growth-phase predictions exhibit a zonal SSTA dipolar pattern, with the western poles (centered in the equatorial central–western Pacific) revealing positive anomalies and the eastern poles (the equatorial eastern Pacific) exhibiting negative anomalies. On the other hand, the NFSV2 errors associated with decaying-phase predictions tend to follow a pattern almost opposite to the NFSV1 errors. Usually, the NFSV1 causes negative prediction errors relative to Niño-3 SSTA in El Niño events, and the NFSV2 is inclined to yield positive prediction errors. Furthermore, the growth-phase predic-

tion uncertainties caused by NFSVs are usually larger than the corresponding uncertainties in the decaying-phase predictions. The resultant prediction errors show a conspicuous season-dependent evolution, with the fastest error growth occurring in the AMJ and/or JAS seasons. That is, the NFSV tendency errors, which cause the largest prediction errors at the time of the prediction, induce a prominent season-dependent evolution in those errors and therefore lead to a significant SPB to El Niño events.

Although the FSV tendency errors possess patterns similar to the corresponding NFSV errors, their western poles are centered much farther eastward and cause smaller prediction errors. Meanwhile, the prediction errors caused by FSVs demonstrate smaller growth rates during the AMJ/JAS season, and hence yield a less significant SPB. Moreover, we also show that random tendency errors without a particular structure yield negligible prediction errors; and their evolution is not significantly seasonal. Therefore, random tendency errors do not cause the SPB phenomenon. These results imply that the SPB to El Niño predictions is closely linked to the spatial structure of tendency errors, and a particular tendency error similar to an NFSV could induce a significant SPB.

NFSVs often concentrate the tendency errors of large values in a few areas within the eastern equatorial Pacific and the central–western equatorial Pacific; thus, these areas may have a much larger effect on prediction uncertainties than other areas. Therefore, these regions may be sensitive to model errors relative to El Niño predictions. That is, if we improve the model simulations in these sensitive areas compared to those in other areas, its ENSO forecast ability more likely to be greatly improved. As for the sensitive areas determined by the FSVs, they are somewhat different from those obtained by using the NFSVs. However, FSVs are obtained from an approximate tangent linear model of a nonlinear model, and the process itself induces model error; on the other hand, NFSVs are developed directly from a nonlinear model without any approximation. Therefore, the results obtained from NFSVs are more convincing. Certainly, additional sensitivity experiments and even hindsight experiments are needed to verify the sensitive areas identified by the NFSVs, and our results should be confirmed by using a more realistic ENSO model.

Yu et al. (2012b) used the Zebiak–Cane model to demonstrate that the equatorial central–eastern Pacific and eastern Pacific represent the areas where ENSO predictions are sensitive to initial errors, which are exactly those areas identified in this study as being associated with model errors characterized by NFSVs. Accordingly, additional data using target observations in the sensitive areas will not only provide a more accurate initial field of information but also improve our understanding of ENSO physics to optimize ENSO models and thus improve ENSO forecasting accuracy greatly.

In the end, the present study shows that the model errors represented by NFSV tendency errors can cause a significant SPB phenomenon associated with El Niño event prediction. These NFSV tendency errors could also be excited by atmospheric noise forcing (Yu et al., 2003; Gebbie and Tziperman, 2009; Lopez and Kirtman, 2014). As such, relevant experiments should be conducted to test these mechanisms in the future. In addition, previous studies such as Mu et al. (2007a, b), Duan et al. (2009), and Yu et al. (2009) have demonstrated that CNOP-related initial errors induce a significant SPB. In realistic ENSO predictions, initial errors coexist with model errors. Thus, it is necessary to explore the relative role of initial errors and model errors and their interactions in generating a significant SPB to ENSO prediction, which we have begun to address here. Finally, we note that the El Niño events generated by the Zebiak–Cane model are characterized by a decaying period that is too long, which indicates that the termination of an El Niño event does not occur in spring (Stuecker et al., 2013, 2015), which may limit the results in this study. Some studies have argued that the occurrence of an SPB in ENSO event prediction relates to the fact that the weakest ENSO signal occurs during spring (Xue et al., 1994; Samelson and Tziperman, 2001). Although the termination of El Niño in the Zebiak–Cane model is not in spring, the predictions generated by the

Zebiak–Cane model still yield an SPB for ENSO. This indicates that the occurrence of an SPB in this model may not be due to a weak ENSO signal in spring. Of course, this inference should be confirmed by numerous quantitative experiments in future works. In any cases, the results obtained from the present work are expected to be enlightening for further investigation.

REFERENCES

Barkmeijer, J., T. Iversen, and T. N. Palmer, 2003: Forcing singular vectors and other sensitive model structures. *Quart. J. Roy. Meteor. Soc.*, **129**, 2401–2423.

Blanke, B., J. D. Neelin, and D. Gutzler, 1997: Estimating the effect of stochastic wind stress forcing on ENSO irregularity. *J. Climate*, **10**, 1473–1486.

Blumenthal, M. B., 1991: Predictability of a coupled ocean–atmosphere model. *J. Climate*, **4**, 766–784.

Chen, D. K., S. E., Zebiak, A. J. Busalacchi, et al., 1995: An improved procedure for El Niño forecasting: Implications for predictability. *Science*, **269**, 1699–1702.

Chen, D. K., M. A. Cane, A. Kaplan, et al., 2004: Predictability of El Niño over the past 148 years. *Nature*, **428**, 733–736.

Dommenget, D., and Y. S. Yu, 2016: The seasonally changing cloud feedbacks contribution to the ENSO seasonal phase-locking. *Climate Dyn.*, doi: 10.1007/s00382-016-3034-6.

Dommenget, D., T., Bayr, and C. Frauen, 2013: Analysis of the non-linearity in the pattern and time evolution of El Niño–Southern Oscillation. *Climate Dyn.*, **40**, 2825–2847.

Duan Wansuo and Zhang Rui, 2010: Is model parameter error related to a significant spring predictability barrier for El Niño events? Results from a theoretical model. *Adv. Atmos. Sci.*, **27**, 1003–1013.

Duan, W. S., and C. Wei, 2012: The "spring predictability barrier" for ENSO predictions and its possible mechanism: Results from a fully coupled model. *Int. J. Climatol.*, **33**, 1280–1292, doi: 10.1002/joc.3513.

Duan, W. S., and F. F. Zhou, 2013: Non-linear forcing singular vector of a two-dimensional quasi-geostrophic model. *Tellus A*, **65**, 18452.

Duan, W. S., and P. Zhao, 2015: Revealing the most disturbing tendency error of Zebiak–Cane model associated with El Niño predictions by nonlinear forcing singular vector approach. *Climate Dyn.*, **44**, 2351–2367, doi: 10.1007/s00382-014-2369-0.

Duan, W. S., and J. Y. Hu, 2016: The initial errors that induce a significant "spring predictability barrier" for El Niño events and their implications for target observation: Results from an earth system model. *Climate Dyn.*, **46**, 3599–3615, doi: 10.1007/s00382-015-2789-5.

Duan, W. S., X. C. Liu, K. Y. Zhu, et al., 2009: Exploring the initial errors that cause a significant "spring predictability barrier" for El Niño events. *J. Geophys. Res.*, **114**, C04022, doi: 10.1029/2008JC004925.

Flügel, M., and P. Chang, 1998: Does the predictability of ENSO depend on the seasonal cycle? *J. Atmos. Sci.*, **55**, 3230–3243.

Gebbie, G., and E. Tziperman, 2009: Predictability of SST-modulated westerly wind bursts. *J. Climate*, **22**, 3894–3909.

Jin, E. K., J. L. Kinter III, B. Wang, et al., 2008: Current status of ENSO prediction skill in coupled ocean–atmosphere models. *Climate Dyn.*, **31**, 647–664.

Kirtman, B. P., J. Shukla, M. Balmaseda, et al., 2002: Current status of ENSO forecast skill: A report to the climate variability and predictability (CLIVAR) Numerical Experimentation Group (NEG). CLIVAR Working Group on seasonal to interannual prediction, 31 pp. (Available online at http://www.cliver.org/publications/wgpreports/wgsip/nino3/report.html.)

Kleeman, R., 1991: A simple model of the atmospheric response to ENSO sea surface temperature anomalies. *J. Atmos. Sci.*, **48**, 3–19.

Latif, M., D. Anderson, T. Barnett, et al., 1998: A review of the predictability and prediction of ENSO. *J. Geophys. Res.*, **103**, 14375–14393.

Latif, M., T. P. Barnett, M. A. Cane, et al., 1994: A review of ENSO prediction studies. *Climate Dyn.*, **9**, 167–179.

Lau, K. M., and S. Yang, 1996: The Asian monsoon and predictability of the tropical ocean–atmosphere system. *Quart. J. Roy. Meteor. Soc.*, **122**, 945–957.

Levine, A. F. Z., and M. J., McPhaden, 2015: The annual cycle in ENSO growth rate as a cause of the spring predictability barrier. *Geophys. Res. Lett.*, **42**, 5034–5041.

Liu, Z. Y., 2002: A simple model study of ENSO suppression by external periodic forcing. *J. Climate*, **15**, 1088–1098.

Lopez, H., and B. P. Kirtman, 2014: WWBs, ENSO predictability, the spring barrier and extreme events. *J. Geophys. Res.*, **19**, 10114–10138, doi: 10.1002/2014JD021908.

Luo, J. J., S. Masson, S. K. Behera, et al., 2008: Extended ENSO predictions using a fully coupled ocean–atmosphere model. *J. Climate*, **21**, 84–93.

Marshall, A. G., O. Alves, and H. H. Hendon, 2009: A coupled GCM analysis of MJO activity at the onset of El Niño. *J. Atmos. Sci.*, **66**, 966–983.

McCreary, J. P. Jr., and D. L. T. Anderson, 1991: An overview of coupled ocean–atmosphere models of El Niño and the Southern Oscillation. *J. Geophy. Res.*, **96**, 3125–3150.

McPhaden, M. J., 2003: Tropical Pacific Ocean heat content variations and ENSO persistence barriers. *Geophys. Res. Lett.*, **30**, 1480, doi: 10.1029/2003GL016872.

McPhaden, M. J., S. E. Zebiak, and M. H. Glantz, 2006: ENSO as an integrating concept in earth science. *Science*, **314**, 1740–1745.

Moore, A. M., and R. Kleeman, 1996: The dynamics of error growth and predictability in a coupled model of ENSO. *Quart. J. Roy. Meteor. Soc.*, **122**, 1405–1446.

Mu Mu, Duan Wansuo, and Wang Jiacheng, 2002: The predictability problems in numerical weather and climate prediction. *Adv. Atmos. Sci.*, **19**, 191–204.

Mu, M., W. S. Duan, and B. Wang, 2003: Conditional nonlinear optimal perturbation and its applications. *Nonlinear Processes in Geophysics*, **10**, 493–501.

Mu, M., H. Xu, and W. S. Duan, 2007a: A kind of initial errors related to "spring predictability barrier" for El Niño events in Zebiak–Cane model. *Geophys. Res. Lett.*, **34**, L03709, doi: 10.1029/2006GL-27412.

Mu, M., W. S. Duan, and B. Wang, 2007b: Season-dependent dynamics of nonlinear optimal error growth and El Niño–Southern Oscillation predictability in a theoretical model. *J. Geophys. Res.*, **112**, D10113, doi: 10.1029/2005JD006981.

Mu, M., Y. S. Yu, H. Xu, et al., 2014: Similarities between optimal precursors for ENSO events and optimally growing initial errors in El Niño predictions. *Theor. Appl. Climatol.*, **115**, 461–469. doi: 10.1007/s00704-013-0909-x.

Penland, C, and T. Magorian, 1993: Prediction of Niño 3 sea surface temperatures using linear inverse modeling. *J. Climate*, **6**, 1067–1076.

Roads, J. O., 1987: Predictability in the extended range. *J. Atmos. Sci.*, **44**, 3495–3527.

Samelson, R. M., and E. Tziperman, 2001: Instability of the chaotic ENSO: The growth-phase predictability barrier. *J. Atmos. Sci.*, **58**, 3613–3625.

Stein, K., N. Schneider, A. Timmermann, et al., 2010: Seasonal synchronization of ENSO events in a linear stochastic model. *J. Climate*, **23**, 5629–5643.

Stuecker, M. F., A. Timmermann, F. F. Jin, et al., 2013: A combination mode of the annual cycle and the El Niño/Southern Oscillation. *Nature Geoscience*, **6**, 540–544.

Stuecker, M. F., F. F. Jin, A. Timmermann, et al., 2015: Combination mode dynamics of the anomalous northwest pacific anticyclone. *J. Climate*, **28**, 1093–1111.

Syu, H. H., and J. D. Neelin, 2000: ENSO in a hybrid coupled model. Part I: Sensitivity to physical parametrizations. *Climate Dyn.*, **16**, 19–34.

Tang, Y. M., R. Kleeman, and A. M. Moore, 2008: Comparison of information-based measures of forecast uncertainty in ensemble ENSO prediction. *J. Climate*, **21**, 230–247.

Torrence, C., and P. J. Webster, 1998: The annual cycle of persistence in the El Niño/Southern Oscillation. *Quart. J. Roy. Meteor. Soc.*, **124**, 1985–2004.

Webster, P. J., 1995: The annual cycle and the predictability of the tropical coupled ocean–atmosphere system. *Meteor. Atmos. Phys.*, **56**, 33–55.

Webster, P. J., and S. Yang, 1992: Monsoon and ENSO: Selectively interactive systems. *Quart. J. Roy. Meteor. Soc.*, **118**, 877–926.

Williams, P. D., 2005: Modelling climate change: The role of unresolved processes. Philos. *Trans. Roy. Soc. London*, **363**, 2931–2946.

Wu, D. H., D. L. T. Anderson, and M. K. Davey, 1993: ENSO variability and external impacts. *J. Climate*, **6**, 1703–1717.

Xue, Y., M. A. Cane, S. E. Zebiak, et al., 1994: On the prediction of ENSO: A study with a low-order Markov model. *Tellus A*, **46**, 512–528.

Yu, L. S., R. A. Weller, and W. T. Liu, 2003: Case analysis of a role of ENSO in regulating the generation of westerly wind bursts in the western equatorial Pacific. *J. Geophys. Res.*, **108**, 3128, doi: 10.1029/2002JC001498.

Yu, Y. S., W. S. Duan, H. Xu, et al., 2009: Dynamics of nonlinear error growth and season-dependent predictability of El Niño events in the Zebiak–Cane

model. *Quart. J. Roy. Meteor. Soc.*, **135**, 2146–2160.

Yu, Y. S., M. Mu, and W. S. Duan, 2012a: Does model parameter error cause a significant "Spring Predictability Barrier" for El Niño events in the Zebiak–Cane Model? *J. Climate*, **25**, 1263–1277.

Yu, Y. S., M. Mu, W. S. Duan, et al., 2012b: Contribution of the location and spatial pattern of initial error to uncertainties in El Niño predictions. *J. Geophys. Res.*, **117**, C06018, doi: 10.1029/2011JC007758.

Zavala-Garay, J., A. M. Moore, and R. Kleeman, 2004: Influence of stochastic forcing on ENSO prediction. *J. Geophys. Res.*, **109**, C11007, doi: 10.1029/2004JC002406.

Zebiak, S. E., and M. A. Cane, 1987: A model El Niño–Southern Oscillation. *Mon. Wea. Rev.*, **115**, 2262–2278.

Zhang, R. H., S. E. Zebiak, R. Kleeman, et al., 2003: A new intermediate coupled model for El Niño simulation and prediction. *Geophys. Res. Lett.*, **30**, doi: 10.1029/2003GL018010.

Zheng, F., and J. Zhu., 2010: Coupled assimilation for an intermediated coupled ENSO prediction model. *Ocean Dynamics*, **60**, 1061–1073.